The Astronomical Journal, 134:2340–2352, 2007 December

THE STELLAR POPULATIONS OF PRAESEPE AND COMA BERENICES

Adam L. Kraus and Lynne A. Hillenbrand
Department of Astrophysics, California Institute of Technology, MC 105-24, Pasadena, CA 91125, USA; alk@astro.caltech.edu, lah@astro.caltech.edu
Received 2007 July 19; accepted 2007 August 22

ABSTRACT

We present the results of a stellar membership survey of the nearby open clusters Praesepe and Coma Berenices. We have combined archival survey data from the SDSS, 2MASS, USNOB1.0, and UCAC-2.0 surveys to compile proper motions and photometry for ~5 million sources over 300 deg^2. Of these sources, 1010 stars in Praesepe and 98 stars in Coma Ber are identified as candidate members with probability >80%; 442 and 61 are identified as high-probability candidates for the first time. We estimate that this survey is >90% complete across a wide range of spectral types (F0–M5 in Praesepe, F5–M6 in Coma Ber). We have also investigated the stellar mass dependence of each cluster's mass and radius in order to quantify the role of mass segregation and tidal stripping in shaping the present-day mass function and spatial distribution of stars. Praesepe shows clear evidence of mass segregation across the full stellar mass range; Coma Ber does not show any clear trend, but low number statistics would mask a trend of the same magnitude as in Praesepe. The mass function for Praesepe ($\tau \sim 600$ Myr; $M \sim 500\ M_\odot$) follows a power law consistent with that of the field present-day mass function, suggesting that any mass-dependent tidal stripping could have removed only the lowest mass members ($<0.15\ M_\odot$). Coma Ber, which is younger but much less massive ($\tau \sim 400$ Myr; $M \sim 100\ M_\odot$), follows a significantly shallower power law. This suggests that some tidal stripping has occurred, but the low-mass stellar population has not been strongly depleted down to the survey completeness limit ($\sim 0.12\ M_\odot$).

Key words: open clusters and associations: individual (Praesepe, Coma Berenices) — stars: evolution — stars: fundamental parameters — stars: luminosity function, mass function

Online material: color figures, machine-readable tables

1. INTRODUCTION

Star clusters are among the most powerful and versatile tools available to stellar astronomy. Nearby clusters serve as prototypical populations for studying many diverse topics of stellar astrophysics, including star formation, stellar structure, stellar multiplicity, and circumstellar processes like planet formation (e.g., Patience et al. 2002; Bouy et al. 2006; Muench et al. 2007; Stauffer et al. 2007; Siegler et al. 2007); star clusters are uniquely sensitive to the physics of these processes due to their uniform and well-constrained age, distance, and metallicity. Open clusters are also thought to be the birthplaces of most stars, so the formation, evolution, and disruption of clusters establish the environment of star formation and early stellar evolution. Two of the nearest open clusters are Praesepe and Coma Berenices. Praesepe is a rich ($N \sim 1000$ known or suspected members), intermediate-age (~600 Myr) cluster at a distance of 170 pc (Hambly et al. 1995a), while Coma Ber is younger and closer (~400 Myr; 90 pc) and much sparser ($N \sim 150$; Casewell et al. 2006).

Praesepe has been the target of numerous photometric and astrometric membership surveys over the past century; part of the reason for its popularity is that its proper motion is relatively distinct from that of field stars (-36.5, -13.5 mas yr^{-1}), simplifying the identification of new members. Its high-mass stellar population was identified early in the last century by Klein-Wassink (1927), and subsequent surveys extended the cluster census to intermediate-mass stars (Artyukhina 1966; Jones & Cudworth 1983). The M dwarf stellar population was first identified by Jones & Stauffer (1991). A later survey by Hambly et al. (1995a) extended this work to a fainter limit and a larger fraction of the cluster, producing a cluster census that is still used for most applications (e.g., Allen & Strom 1995; Holland et al. 2000; Kafka & Honeycutt 2006). There have been additional surveys to identify cluster members, but they have been prone to contamination from field stars (Adams et al. 2002) or based purely on photometry with no astrometric component (Pinfield et al. 1997; Chappelle et al. 2005).

Coma Ber, in contrast, has been largely neglected in surveys of nearby open clusters. The cluster would be an ideal population for many studies due to its proximity (second only to the Hyades) and intermediate age between the Pleiades (125 Myr) and Hyades or Praesepe (~600 Myr), but its members are difficult to distinguish from field stars because it has a proper motion (-11.5, -9.5 mas yr^{-1}) which is significantly lower than that of Praesepe. It is also a much sparser cluster than Praesepe, and its few members are projected over a much larger area of the sky. Its high-mass stellar population has been known for many decades (Trumpler 1938), but only a handful of additional members have been confirmed (Artyukhina 1966; Argue & Kenworthy 1969; Bounatiro 1993; Odenkirchen et al. 1998); many candidate members have been identified, but a large fraction of them have been shown to be unrelated field stars (e.g., Jeffries 1999; Ford et al. 2001). One survey for low-mass stars was conducted recently by Casewell et al. (2006), who used 2MASS photometry and USNO-B1.0 astrometry to identify 60 candidate members extending well into the M dwarf regime (~0.30 $M_\odot$). This survey discovered many candidate members with spectral types of late G and early M, but, as we discuss later, significant contamination from field stars rendered it completely insensitive to *K* dwarf members and diluted its other discoveries with a significant number of nonmembers.

In this paper we combine the photometric and astrometric results of several wide-field imaging surveys to compile a full

stellar census of Praesepe and Coma Ber. This census is both wider and deeper than any previous proper-motion survey, extending to near the substellar boundary. Our results for Praesepe allow us to fully characterize the structure and dynamical evolution of this prototypical cluster, while our results for Coma Ber unveil a new benchmark stellar population that is closer than any cluster except the Hyades and that fills a poorly studied age range. In § 2 we describe the all-sky surveys that contribute to our cluster census, and in § 3 we describe the photometric and astrometric analysis techniques that we used to identify new members. We summarize our new catalog of cluster members in § 4. Finally, in § 5, we analyze the structure and properties of each cluster.

2. DATA SOURCES

In this survey, we worked with archival data from several publicly available surveys: SDSS, 2MASS, USNO-B1.0, and UCAC2. In each case we extracted a portion of the source catalog from the data access Web sites. We worked with circular areas of radius 7° centered on the core of each cluster (8^h40^m, +20° and 11^h24^m, +26°, respectively); for both clusters, this radius is approximately twice the estimated tidal radius (Hambly et al. 1995a; Casewell et al. 2006).

2.1. *SDSS*

The Sloan Digital Sky Survey (SDSS; York et al. 2000) is an ongoing deep optical imaging and spectroscopic survey of the northern galactic cap. The most recent data release (DR5; Adelman-McCarthy et al. 2006) reported imaging results in five filters (*ugriz*) for 8000 deg^2, including the full areas of Praesepe and Coma Ber. The 10 σ detection limits in each filter are $u = 22.0$, $g = 22.2$, $r = 22.2$, $i = 21.3$, and $z = 20.5$; the saturation limit in all filters is $m \sim 14$. The typical absolute astrometric accuracy is ~45 mas rms for sources brighter than $r = 20$, declining to 100 mas at $r = 22$ (Pier et al. 2003); absolute astrometry was calibrated with respect to stars from UCAC2, which is calibrated to the Inertial Coordinate Reference Frame (ICRS).

The default astrometry reported by the SDSS catalog is the *r*-band measurement, not the average of all five filters. However, the residuals for each filter (with respect to the default value) are available, so we used these residuals to construct a weighted mean value for our analysis. We adopted a conservative saturation limit of $m \sim 15$ in all filters, even though the nominal saturation limit is $m \sim 14$, because we found that many photometric measurements were mildly saturated for $14 < m < 14.5$. We also neglect measurements which are flagged by the SDSS database as having one or more saturated pixels. Finally, we removed all sources which did not have at least one measurement above the nominal 10 σ detection limits. Any cluster members fainter than this limit will not have counterparts in other catalogs, and the presence of excess sources can complicate attempts to match counterparts between data sets.

2.2. *USNO-B1.0*

The USNO-B1.0 survey (USNOB; Monet et al. 2003) is a catalog based on the digitization of photographic survey plates from five epochs. For fields in the north, including both Praesepe and Coma Ber, these plates are drawn from the two Palomar Observatory Sky Surveys, which observed the entire northern sky in the 1950s with photographic *B* and *R* plates and the 1990s with photographic *B*, *R*, and *I* plates; we follow standard USNOB nomenclature in designating these observations *B*1, *R*1, *B*2, *R*2, and *I*2.

The approximate detection limits of the USNOB catalog are $B \sim 20$, $R \sim 20$, and $I \sim 19$, and the observations saturate for stars brighter than $V \sim 11$. The typical astrometric accuracy at each epoch is ~120 mas, albeit with a significant systematic uncertainty (up to 200 mas) due to its uncertain calibration into the ICRS via the unpublished USNO YS4.0 catalog. As we describe in § 3.2, we have recalibrated the USNOB astrometry at each epoch using UCAC2 astrometry; this step reduces the systematic uncertainty.

2.3. *2MASS*

2MASS (Skrutskie et al. 2006) observed the entire sky in the *J*, *H*, and K_s bands over the interval of 1998–2002. Each point on the sky was imaged six times and the coadded total integration time was 7.8 s, yielding 10 σ detection limits of $K = 14.3$, $H = 15.1$, and $J = 15.8$. The saturation levels depend on the seeing and sky background for each image, but are typically $J < 9$, $H < 8.5$, and $K_s < 8$. However, the NIR photometry is typically accurate to well above these saturation limits, since it was extrapolated from the unsaturated PSF wings. The typical astrometric accuracy attained for the brightest unsaturated sources ($K \sim 8$) is ~70 mas. The absolute astrometry calibration was calculated with respect to stars from Tycho-2; subsequent tests have shown that systematic errors are typically $\lesssim$30 mas (Zacharias et al. 2003).

2.4. *UCAC2*

The astrometric quality of all three of the above surveys could be compromised for bright, saturated stars, so proper motions calculated from those observations could be unreliable. Many of the brightest stars are saturated in all epochs, so we have no astrometry with which to compute proper motions. We have addressed this problem by adopting proper motions for bright stars as measured by the Second USNO CCD Astrograph Catalog (UCAC2; Zacharias et al. 2004).

UCAC2 was compiled from a large number of photographic sky surveys and a complete reimaging of the sky south of $\delta \sim 40°$. UCAC2 is not complete, since many resolved sources (double stars and galaxies) were rejected. However, most sources between $R = 8$ and 16 should be included. The typical errors in the reported proper motions are ~1–3 mas yr^{-1} down to $R = 12$ and ~6 mas yr^{-1} to $R = 16$. We have adopted UCAC2 proper motions in cases where we were unable to calculate new values or where the UCAC2 uncertainties are lower than the uncertainties for our values.

2.5. *Known Members of Praesepe*

There have been many previous surveys to identify members of Praesepe, so we have compiled a list of high-confidence cluster members that can be used to test our survey procedures (§ 3) and determine the completeness of our survey (§ 4.2). We have not done the same for Coma Ber, since there are far fewer high-confidence members (<50). However, the brightness ranges are similar enough that the detection efficiencies should be similar for both clusters.

We drew our high-confidence Praesepe sample from the proper motion surveys of Jones & Cudworth (1983), Jones & Stauffer (1991), and Hambly et al. (1995a). We also included the high-mass stars identified by Klein-Wassink (1927) which possessed updated astrometry in the survey by Wang et al. (1995). We required each member of our high-confidence sample to have been identified with ≥95% probability of membership by at least one

survey, and to not have been identified with <80% probability by any other survey; a total of 381 sources met these requirements.

3. DATA ANALYSIS

Cluster surveys typically identify candidate members using a combination of photometric and astrometric data. All cluster members have the same age, distance, and 3D spatial velocity, so they follow the same color-magnitude sequence and have the same proper motion. This allows for the efficient rejection of all nonmembers which do not meet both criteria.

In the following subsections we describe our procedure for applying these tests. First, we use SED fitting for our photometric data (spanning 0.3–2.3 μm) to estimate the temperatures and luminosities of all $\sim$5 million sources, and then we calculate a weighted least-squares fit of our time-series astrometric data to calculate the corresponding proper motions. After deriving both sets of results, we then cut the overwhelming majority of sources which do not follow the cluster photometric sequence. Finally, we examine the (much smaller) list of remaining sources and determine membership probabilities based on the level of agreement between individual candidate astrometry (proper motion and radius from cluster center) and the corresponding distributions for the cluster and for background stars.

We chose to apply the cuts in this order specifically because the final membership probabilities are based on the astrometric properties and not the photometric properties, but inverting the order of the cuts would not affect our final results. Both sets of tests were crucial in narrowing the list of candidates. Of the $\sim 10^6$ sources in each cluster for which we measured proper motions, $\sim 10^5$ would have been selected by a purely kinematic test and $\sim 10^4$ would have been selected by a purely photometric test.

3.1. *SED Fitting*

We base our photometric analysis on the merged results from 2MASS and SDSS, which yield measurements in eight filters (*ugrizJHK*) for each source. We do not use the photometric results reported by USNOB because they are much more uncertain ($\sim$0.25 mag) and do not introduce any new information beyond that reported by SDSS. We also note that many high-mass sources were saturated in one or more filters, so they had fewer than eight photometric measurements available; the highest mass stars were saturated in all five SDSS filters, leaving only *JHK* photometry.

Candidate cluster members traditionally have been selected by photometric surveys which measure magnitudes in several bandpasses and then estimate each star's intrinsic properties (bolometric flux and temperature) using its observed properties (magnitudes and colors). Candidate members are then selected from those stars which fall along the cluster sequence (as defined by known members and by theoretical models) on color-magnitude diagrams. However, this method suffers from serious flaws. A single magnitude is typically taken as a proxy for flux, which places excessive weight on that bandpass and underweights other bandpasses in the survey. If there are more than two bandpasses, motivating the use of multiple CMDs, then color-magnitude selection also neglects the covariance between measurements, artificially inflating the uncertainty in an object's intrinsic properties. Finally, the use of many CMDs introduces significant complexity in the interpretation and communication of results.

We have addressed these challenges by developing a new method for photometric selection of candidate members. Instead of using many different combinations of color and magnitude as proxies for stellar flux and temperature, we have used an SED-fitting routine to estimate directly each star's intrinsic properties, then selected candidate members based on their positions in the resulting H-R diagram. This method is not vulnerable to the flaws of individual color-magnitude selection since it uses all data simultaneously and uniformly, and since we can implement it as a least-squares minimization, it significantly reduces the uncertainty in the final results.

Specifically, for each star we calculated the χ^2 goodness of fit for the system of eight equations:

$$M_i - m_i = \mathrm{DM},$$

where m_i is the observed magnitude in filter i, M_i is the absolute magnitude in filter i for the SED model being tested, and DM is the distance modulus, which was estimated from a weighted least-squares fit across all filters. This system ignores the effects of reddening, but this should be minimal for both clusters. Taylor (2006) found a reddening value for Praesepe of $E(B-V) = 27 \pm 4$ mmag, while Feltz (1972) found a value for the Coma Ber region of $E(B-V) = 0 \pm 2$ mmag.

We tested a library of 491 stellar SEDs which spanned a wide range of spectral types: B8–L0, in steps of 0.1 subclasses. We describe the SED library and its construction in more detail in the Appendix. We rejected potentially erroneous observations by rejecting any measurement that disagreed with the best-fit SED by more than 3 σ, where σ is the photometric error reported by the SDSS or 2MASS, and then calculating a new fit. The model which produced the best χ^2 fit over the eight filters was adopted as the object spectral type, and the corresponding value of DM was added to the model's absolute bolometric magnitude to estimate the apparent bolometric flux. The uncertainties in the spectral type and distance modulus were estimated from the 1 σ interval of the χ^2 fit for each object.

In Figure 1 (*left*) we plot an H-R diagram for our high-confidence sample of Praesepe members. The middle line shows the field main sequence at the distance of Praesepe (see the Appendix), and the outer lines show the upper and lower limits that we use for identifying cluster members. For stars earlier than M2, these limits are set 0.5 mag below and 1.5 mag above the main sequence to allow for the width of the cluster sequence (due to errors, the finite depth of the cluster, and the existence of a multiple-star sequence). The late main sequence is nearly vertical in the H-R diagram, which suggests that uncertainties in spectral type will be more important than uncertainties in flux for broadening the cluster sequence. We account for this by extending the selection range for spectral types $\geq$M2 to 0.7 mag below and 1.7 mag above the field main sequence. Most of the 15 outliers have fluxes or spectral types that are biased by one or more photometric measurements which appear to be erroneous by less than 3 σ, causing them to fall just outside our selection range. However, four sources appear to have colors and magnitudes that are genuinely inconsistent with the cluster sequence.

In Figure 2 we plot our photometric spectral type against previously measured spectroscopic spectral types for 632 candidate Praesepe members (Ramberg 1938; Bidelman 1956; Corbally & Garrison 1986; Abt 1986; Williams et al. 1994; Allen & Strom 1995; Adams et al. 2002; Kafka & Honeycutt 2006). The two sets of spectral types agree systematically to within <2 subclasses; the dispersion in the relation is $\sim$3 subclasses for early-type stars (A0–G0) and $\lesssim$1 subclass for later type stars (G0–M6). This dispersion represents the combined dispersions of both our measurements and those in the literature, so it represents an upper limit on the statistical uncertainties in our spectral

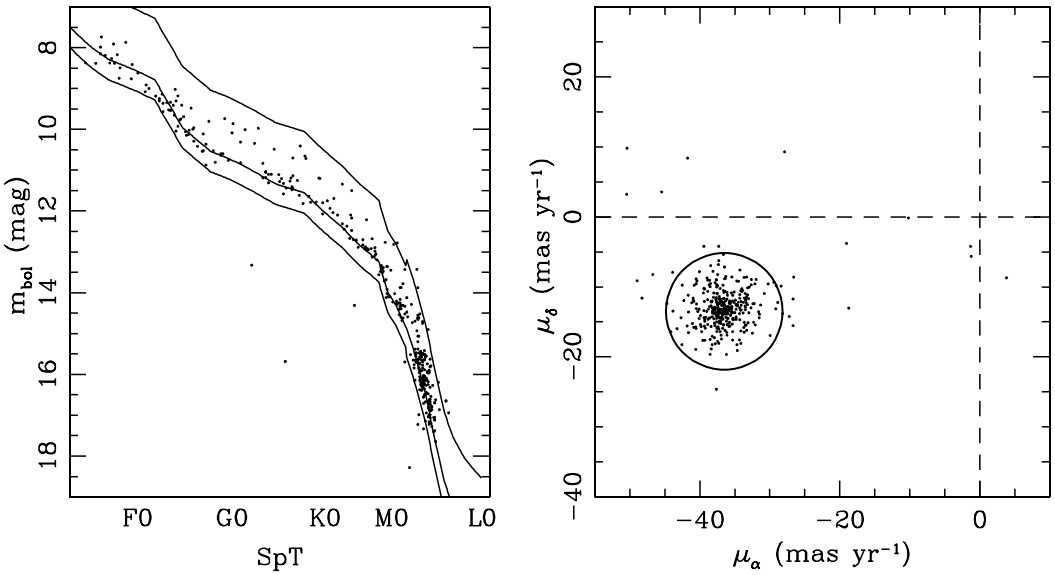

FIG. 1.—H-R (*left*) and proper-motion (*right*) diagrams for our high-confidence sample of Praesepe members. For the H-R diagram, we plot the cluster single-star sequence (*middle line*) and the selection range for identifying new members (*outer lines*). In the proper-motion diagram, we plot a circle of radius 8 mas yr^{-1} (approximately 2 σ for a typical M4 member) centered at the mean cluster proper motion. [*See the electronic edition of the Journal for a color version of this figure.*]

type estimate. Most of the early-type stars were classified by Ramberg and Bidelman, so the larger scatter could be a result of their older, less precise observing techniques. However, our SED-fitting routine rejected most of the SDSS photometry for these sources since it was saturated, so some of the uncertainty may be a result of using only 2MASS *JHK* photometry.

When applied to our full source list, our photometric selection criteria identify 11,999 candidate members of Praesepe and 2034 candidate members of Coma Ber. As we demonstrate in the §§ 3.2 and 3.3, the vast majority of these sources are probably background stars, since they have proper motions inconsistent with cluster membership.

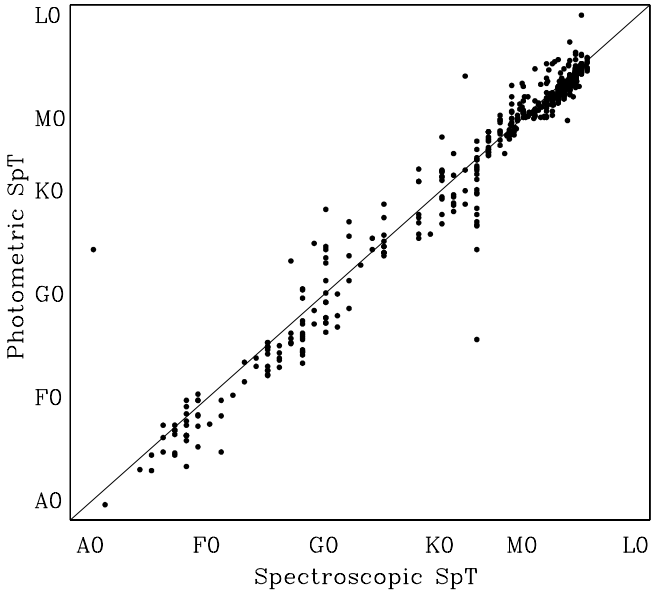

FIG. 2.—Comparison of our photometric spectral type determinations to spectroscopic determinations for 632 candidate Praesepe members in the literature. The small excess of points below the relation at spectral type K3 are all drawn from the spectroscopic survey of Adams et al. (2002), which observed spectra in a red wavelength range that contained no diagnostics for distinguishing FGK stars. The A0 star that we misclassified (KW 552) is an Algol-type eclipsing binary, so the 2MASS photometry may have been obtained during primary eclipse; we did not use any SDSS photometry in its SED fit because it was all saturated. If this is the case, our derived spectral type corresponds to an unknown combination of light from the primary and secondary. The K2 star that we misclassified (KW 572) was biased by saturated SDSS photometry which was not flagged.

3.2. *Proper Motions*

Kinematic measurements are a key tool in identifying members of stellar populations. Internal cluster velocity dispersions are typically much lower than the dispersion of field star velocities, so stellar populations generally can be distinguished from the field star population by their uniform kinematics. The measurement of tangential kinematics, via proper motions, is also an efficient method, since it can be applied to many cluster members simultaneously using wide-field imaging. Many recent efforts have employed various combinations of all-sky surveys in order to systematically measure proper motions of both clusters and field stars; USNOB is itself a product of such analysis, and Gould & Kohlmeier (2004) produced an astrometric catalog for the overlap between USNOB and SDSS Data Release 1. However, there has been no systematic attempt to combine all available catalogs using a single algorithm to produce a single unified set of kinematic measurements.

Before calculating proper motions for our survey, our first step was to recalibrate the five epochs of USNOB astrometry into the ICRS. The densest reference system that is directly tied to the ICRS is UCAC2, which we already cross-referenced with our data set, so we used all of its sources with high-precision astrometry ($\sigma_\mu \lesssim$ 4 mas yr^{-1}) as calibrators. For each USNOB epoch, we projected the simultaneous UCAC2 positions of all calibrators using modern (epoch 2000) UCAC2 astrometry and proper motions, then determined the median offset between the predicted UCAC2 values and the observed USNOB values. These offsets were then added to each USNOB source to bring its astrometry into the ICRS. We list these median offsets in Table 1; each offset was typically calculated from ~3000 sources, and the standard deviation of the mean for each offset was ~3–5 mas. The median offsets were small (<150 mas), so the net change in our calculated final proper motions is $\lesssim$ 3 mas yr^{-1}.

After we recalibrated all surveys into the same reference system, we used a weighted least-squares fit routine to calculate the

TABLE 1
Astrometric Recalibration Offsets

Cluster/Epoch	Δ_α	Δ_δ
Praesepe B1	+42	+97
Praesepe R1	+49	+104
Praesepe B2	+10	−75
Praesepe R2	−2	−78
Praesepe I2	−11	−119
Coma Ber B1	−16	+55
Coma Ber R1	−21	+80
Coma Ber B2	−132	−58
Coma Ber R2	−96	−64
Coma Ber I2	−118	−93

Notes.—Offsets are measured in mas. The typical uncertainty for each offset, as estimated from the standard deviation of the mean, is ∼3–5 mas.

proper motion of each object based on all available astrometry for unsaturated detections. Our algorithm tested the goodness of each fit and rejected all outliers at >3 σ; most of these outliers were found in the photographic survey data, not in 2MASS or SDSS.

In Figure 1 (*right*) we plot a proper-motion diagram for our high-confidence sample of Praesepe members. The mean cluster proper motion (−36.5, −13.5 mas yr^{-1}) is denoted by a circle with a radius of 8 mas yr^{-1} (twice the typical 1 σ uncertainty for the M4 members in our high-confidence sample). We found that 326 of our 381 high-confidence members fall within this limit, and most of the early-type stars (which have much smaller errors) form a much tighter distribution. Most of the outliers appear to be biased by erroneous first-epoch positions that cannot be rejected at a 3 σ level by our fitting routine. These early epochs are not significantly more prone to erroneous measurements than later photographic measurements, but they change the resulting proper motion by a larger amount, since their time baseline with respect to all other measurements is so long.

Our subsequent kinematic analysis (§ 3.3) has retained all photometric candidates with proper motions within 20 mas yr^{-1} (5 σ for low-mass candidates) of each cluster's mean proper motion; we set this limit to be much larger than the cluster distribution so that we would also retain enough field stars to determine their density in proper-motion space. We found that 2611 of our 11,999 photometric candidates in Praesepe and 645 of our 2034 photometric candidates in Coma Ber fell within this limit.

We removed a small number of sources (44 from Praesepe and 4 from Coma Ber) that had highly uncertain proper motions ($\sigma >$ 10 mas yr^{-1}) because we could not have accurately assessed their membership. The astrometry was typically more uncertain for these few sources because there were few or no detections in USNOB. We also visually inspected the SED for any source with a poor photometric fit ($\chi^2_\nu > 10$) and rejected two sources near Coma Ber which were only selected due to saturated SDSS photometry that had not been flagged.

Finally, we visually inspected the color-composite SDSS image of each source using the SDSS batch image service.[1] We found that eight sources in Praesepe and 31 sources in Coma Ber were resolved background galaxies, so we removed them from further consideration. These galaxies were split roughly evenly between bright ($r \sim 14$–16) sources with K star colors and faint ($r \sim 19$) galaxies with red *riz* colors and no *ug* or *JHK* detections; in all cases, the apparent proper motion was caused by a large scatter in the photometric centroids. The SDSS database also includes a morphological classification of whether each object is a star or galaxy that is likely to be more sensitive than visual inspection, but we have found that saturated stars and marginally resolved binaries are often classified as galaxies by the SDSS pipeline, so we chose not to use this parameter in rejecting likely galaxies.

[1] See http://cas.sdss.org/dr5/.

3.3. *Identification of Cluster Members*

Our photometric and astrometric selection criteria do not perfectly reject field stars, so we expect that some fraction of our candidates will actually be interlopers and not cluster members. Many surveys quantify the level of contamination by studying one or more control populations, selected from a nearby volume of kinematic or spatial parameter space. The membership probability for a set of stars is then represented by the fractional excess in the candidate population with respect to the control population. However, this choice ignores all information about the spatial or proper-motion distribution of the candidates, treating these distributions as constant within the selection limits. A more rigorous approach should take these nonconstant probability density functions into account, giving highest membership probability to those candidates that are closest to the cluster center and have proper motions closest to the mean cluster value.

To this end, we have adopted the maximum likelihood method of Sanders (1971) and Francic (1989) to distinguish cluster members and field stars among the candidates that meet our photometric and kinematic selection criteria. This method explicitly fits the spatial and kinematic distributions of all candidates with two separate probability density functions, $\Phi = \Phi_c + \Phi_f$, corresponding to cluster members and field interlopers. The method then assigns a membership probability to each star based on the values of each distribution for that location in parameter space, $P_{\rm mem} = \Phi_c/(\Phi_c + \Phi_f)$.

Following some of the refinements of Francic (1989), we chose to fit the cluster spatial distribution with an exponential function and the cluster proper-motion distribution with a Gaussian function:

$$\Phi_c(\mu_\alpha, \mu_\delta, r) = \frac{N_c e^{-r/r_0}}{2\pi^2 r_0^2 \sigma^2} e^{1/2\sigma^2 \left[(\mu_\alpha - \mu_{\alpha,m})^2 + (\mu_\delta - \mu_{\delta,m})^2\right]},$$

where the quantities N_c (the total number of cluster stars), r_0 (the scale radius), and σ (the standard deviation of the cluster proper-motion distribution) were determined from the fit. We adopted the mean proper motions of each cluster, $(\mu_{\alpha,m}, \mu_{\delta,m}) = (-36.5, -13.5)$ mas yr^{-1} (Praesepe) and $(-11.5, -9.5)$ mas yr^{-1} (Coma Ber), from the literature; these results match UCAC2 values for known high-mass cluster members.

We evaluated the option of fitting the cluster spatial distribution with a mass-dependent King profile (King 1962), but we found that the function produced a poor fit at large separations. High-mass stars in particular are more centrally concentrated than a King profile would predict. By contrast, an exponential radial density profile can accurately match the outer density profile at the cost of moderately overestimating the central density. We decided that it is more important to accurately predict the spatial structure of the outer cluster, where cluster members are less numerous and harder to distinguish from field stars, so we chose to use the exponential profile.

We chose to fit the field spatial distribution with a constant function since the density of field stars does not vary significantly at these high Galactic latitudes. In a departure from previous convention, we also chose to fit the field proper-motion distribution with a constant function. As we show in Figures 4 and 5,

TABLE 2
Cluster Fit Parameters

SpT	N_c	$N_{\rm tot}$	r_0 (deg)	σ (mas yr^{-1})
Praesepe				
A–F	89 ± 9	248	0.45 ± 0.04	1.36 ± 0.10
G	69 ± 8	236	0.49 ± 0.05	1.65 ± 0.14
K0.0–K3.9	72 ± 9	212	0.66 ± 0.09	3.44 ± 0.36
K4.0–K7.9	102 ± 9	247	0.71 ± 0.06	3.34 ± 0.16
M0.0–M1.9	127 ± 9	283	0.71 ± 0.04	2.85 ± 0.16
M2.0–M2.9	90 ± 10	243	0.92 ± 0.10	3.03 ± 0.23
M3.0–M3.9	202 ± 12	440	0.71 ± 0.03	3.01 ± 0.17
M4.0–M4.9	249 ± 15	514	0.87 ± 0.04	4.69 ± 0.28
M5.0–M5.9	40 ± 6	94	0.80 ± 0.10	6.30 ± 0.66
M6.0–M6.9	15 ± 6	42	0.98 ± 0.38	7.00 ± 1.93
Coma Ber				
A–F	17 ± 3	25	1.19 ± 0.24	1.22 ± 0.19
G	13 ± 3	31	1.06 ± 0.16	1.19 ± 0.18
K	40 ± 13	413	1.58 ± 0.17	3.91 ± 0.89
M0.0–M2.9	24 ± 5	50	1.33 ± 0.12	4.58 ± 0.58
M3.0–M5.9	36 ± 6	78	1.46 ± 0.12	5.07 ± 0.58
M6.0–M8.9	3 ± 2	15	1.62 ± 0.55	4.63 ± 1.26

the proper-motion distribution of field stars is not easily parameterized with a single function. However, the distribution varies only on scales much larger than the astrometric precision for typical mid-M candidates ($\sim$4 mas yr^{-1}). If we consider a small region of parameter space, then the distribution should be roughly constant. Thus, the field probability density function we have adopted is

$$\Phi_f = \frac{N_{\rm total} - N_c}{A_{\rm SP} A_{\rm PM}},$$

where $N_{\rm total}$ is the total number of stars (field and cluster), N_c is the number of cluster stars, $A_{\rm SP}$ represents the total spatial area of our survey on the sky (a circle with radius 7°), and $A_{\rm PM}$ represents the total area of proper-motion parameter space from which we selected candidates (a circle with radius 20 mas yr^{-1}). The proper-motion criterion was chosen to be much larger than the typical uncertainty in cluster proper motions ($\sim 5\,\sigma$ for the faintest stars) while being small enough that an assumption of a constant field distribution is approximately valid.

Both clusters are old enough for mass segregation to have occurred, plus the astrometric uncertainties depend significantly on brightness, so we expect that the spatial and kinematic distributions will show a significant mass dependence. We have accounted for this by dividing each cluster sample into spectral type bins and fitting these bins independently. As we describe in § 5, this choice also offers a natural system for quantifying the mass-dependent properties of each cluster. Our parameterization of the cluster spatial and proper-motion distributions provides direct measurements of the cluster mass function (via N_c), the astrometric precision (via σ), and the effects of mass segregation (via r_0).

Finally, we determined confidence intervals for each value via a bootstrap Monte Carlo routine. This method creates synthetic data sets by drawing with replacement from the original data set; for each bin we constructed 100 synthetic data sets with the same number of total members, reran our analysis for each set, and used the distribution of results to estimate the standard deviations of the fit parameters.

In Table 2 we summarize the parameter fits. We found in both clusters that the fits for spectral types >M6 predicted marginally significant values of N_c, a result we attribute to our nondetection of most late-type members. We therefore do not use those parameters in our analysis of the mass-dependent cluster properties. However, in the interest of completeness we still report any candidates which have high membership probabilities. Some of these stars have already been identified as candidates by previous surveys (e.g., IZ 072; Pinfield et al. 2003), so they may be worthy of consideration in future studies. We also found extremely high contamination rates for K stars in Coma Ber; this is a natural result of its low proper motion, which causes confusion with background K giants. There are few high-probability K-type members identified for Coma Ber, but the fits for bulk properties (N_c, r_0, and σ) are statistically significant.

4. RESULTS

4.1. *New Cluster Members*

Based on our kinematic and photometric selection procedures, we identified 1130 candidate members of Praesepe and 149 candidate members of Coma Ber with membership probabilities of $\geq$50%; 1010 and 98 of these candidates have membership probabilities of >80%. Of these high-probability candidates, 76 and 50 are newly identified as proper-motion candidates, while 568 and 37 have been classified as high-probability (>80%) candidates in at least one previous survey, and 366 and 11 were previously identified with lower probability (references in § 1). In Tables 3 and 4, we list all candidate members with $P_{\rm mem} > 50\%$. We also list their derived stellar properties, proper motions, membership probabilities, cross-identifications with previous surveys, and spectroscopically determined spectral types. In Figure 3 we plot a

TABLE 3
Candidate Members of Praesepe

ID	Spectral Type	$m_{\rm bol}$ (mag)	μ_α (mas yr^{-1})	μ_δ (mas yr^{-1})	σ_μ (mas yr^{-1})	$P_{\rm mem}$ (%)	Previous ID[a]
2MASS J08374071+1931064	A8.0 ± 3.2	8.17 ± 0.02	−34.8	−12.5	0.7	99.9	KW 45 (A9; Abt 1986)
2MASS J08430594+1926153	F9.5 ± 3.2	9.74 ± 0.01	−36.6	−13.8	0.9	99.9	KW495 (F8; Ramberg 1938)
2MASS J08393837+1926272	K1.5 ± 1.0	12.10 ± 0.01	−33.0	−9.6	1.9	99.2	KW198 (K3; Allen & Strom 1995)
2MASS J08325566+1843582	K3.3 ± 0.5	12.63 ± 0.01	−38.1	−12.1	3.0	97.1	JS 17
2MASS J08380730+2026557	M1.5 ± 0.1	14.59 ± 0.01	−41.4	−13.2	3.0	99.5	
2MASS J08455917+1915127	M3.5 ± 0.1	15.56 ± 0.01	−41.8	−11.0	2.7	96.6	AD 3470 (M4; Adams et al. 2002)
2MASS J08410334+1837159	M6.8 ± 0.2	17.47 ± 0.01	−37.3	−14.2	4.0	96.5	IZ072 (M4.5; Adams et al. 2002)

Notes.—Table 3 is published in its entirety in the electronic edition of the *Astronomical Journal*. A portion is shown here for guidance regarding its form and content.
[a] The survey by Adams et al. (2002) used standard 2MASS names for their sources. We already provide these names in the first column, so we have labeled the sources as AD *NNNN* (where *NNNN* represents the number of the entry in their results table) in the interest of brevity.

TABLE 4
CANDIDATE MEMBERS OF COMA BER

ID	Spectral Type	m_{bol} (mag)	μ_α (mas yr^{-1})	μ_δ (mas yr^{-1})	σ_μ (mas yr^{-1})	P_{mem} (%)	Previous ID[a]
2MASS J12230841+2551049.....	F9.7±2.9	8.97±0.01	−10.0	−8.5	0.7	100.0	Tr 97 (F8; Abt & Levato 1977)
2MASS J12272068+2319475.....	G7.9±1.5	9.91±0.01	−11.6	−8.8	0.7	99.6	CJD 6 (K0; SIMBAD)
2MASS J12262402+2515430.....	K2.8±0.5	11.55±0.02	−15.9	−6.1	1.7	84.9	
2MASS J12225942+2458584.....	K5.4±0.7	10.86±0.02	−8.7	−12.3	0.9	89.5	
2MASS J12241088+2359362.....	M2.2±0.1	14.03±0.01	−9.9	−9.4	2.7	98.1	CJD 46
2MASS J12163730+2653582.....	M2.6±0.1	14.04±0.01	−7.8	−10.9	3.0	97.6	CJD 45

NOTES.—Table 4 is published in its entirety in the electronic edition of the *Astronomical Journal*. A portion is shown here for guidance regarding its form and content.
[a] The survey by Casewell et al. (2006) did not give explicit names for their sources, so we have labeled the sources as CJD *NN* (where *NN* represents the number of the entry in their results table).

histogram of the number of candidates as a function of P_{mem} for each cluster; a majority of candidates have membership probabilities of >90% or <10%, suggesting that most of these candidates are being unambiguously identified.

To demonstrate the impact of our selection techniques, in Figure 4 we plot an H-R diagram for all stars near Praesepe which fall within 2 σ of the mean cluster proper motion (*left*) and a proper-motion diagram for all stars which passed our photometric selection criteria (*right*). In both cases, the distribution of cluster members can be visually distinguished from the underlying distribution of field stars. However, there is also significant overlap between cluster members and field stars, indicating that both tests were necessary. The proper-motion test was a far better discriminant against field stars, a result of Praesepe's high and distinct proper motion; the photometric criteria accepted 11,999 sources, but only 1932 stars fell within 2 σ of the cluster's mean proper motion.

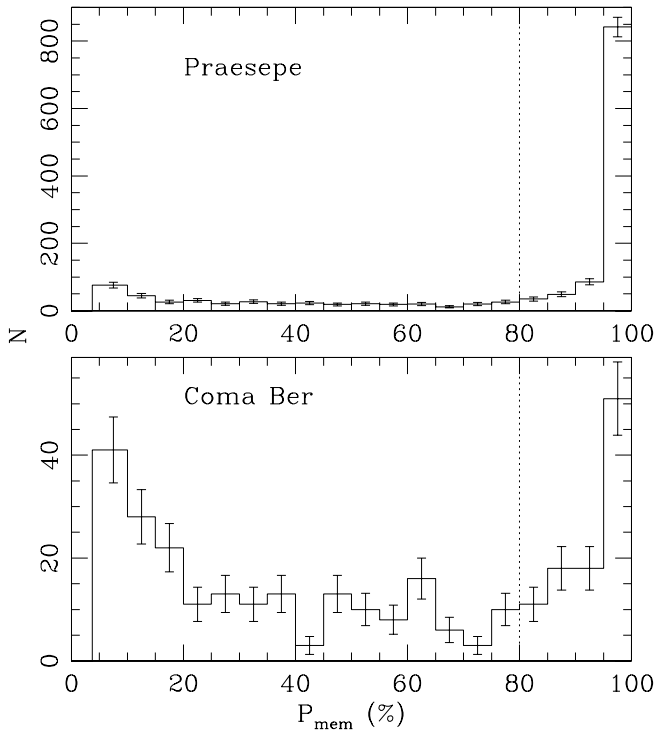

FIG. 3.—Number of candidate members with membership probability P_{mem} for Praesepe (*top*) and Coma Ber (*bottom*). Most of the Coma Ber candidates with $20\% < P_{mem} < 80\%$ are K stars, corresponding to the large number of candidates which we cannot conclusively distinguish as either K dwarf members or background K giant contaminants. The vertical dashed line denotes our suggested limit ($P_{mem} > 80\%$) for identifying high-confidence cluster members.

Based on the H-R diagram, it appears that most field stars with consistent proper motions are nearby dwarfs; this is not surprising, since few distant stars will have the large transverse velocities required to match the angular velocity of Praesepe. Based on the proper-motion diagram, it appears that the interlopers which pass our photometric criteria are split evenly between stationary sources (such as halo giants) and moving sources with larger, randomly distributed proper motions (disk dwarfs that occupy the same physical volume as Praesepe). We also note that a clear binary sequence can be seen for early-type stars in the H-R diagram, but it blends with the single-star sequence for late-type stars ($\gtrsim$M0).

In Figure 5 we plot similar H-R and proper-motion diagrams for the stars of Coma Ber. The cluster's H-R sequence and proper-motion distribution are not as visually distinctive since the cluster population is smaller, but the combination of kinematics and photometry still allow for the efficient identification of candidate members. Unlike for Praesepe, the photometric test was a better discriminant (accepting 2034 sources) than the proper-motion test (21,264 sources); this is a result of the cluster's lower distance (which places it higher in the H-R diagram relative to the field star population) and much smaller proper motion (which allows more contamination from nonmoving background sources).

The H-R diagram for Coma Ber (which shows kinematically selected sources) includes a recognizable giant branch and many faint (distant) early-type stars, both classes which typically have small proper motions. The proper-motion diagram, which shows photometrically selected stars, includes far fewer sources than Praesepe; again, these are split between nonmoving background giants and nearby disk dwarfs. A probable binary sequence can also be seen for Coma Ber, although it is not as visually distinctive as for Praesepe.

4.2. *Completeness*

As we describe in § 2.5, there have been several previous surveys which identified a large number of high-confidence Praesepe members. The resulting sample of 381 members, comprising all stars which have been identified at $\geq$95% confidence in one survey and at no lower than <80% confidence by any others, can test the completeness of our proposed member list.

Of the 381 known member stars, 22 were too bright to have proper motions in UCAC2, so they were immediately excluded from our cluster survey. This suggests that most of the brightest, highest mass stars in either cluster would not have been identified with our technique. Of the 359 stars which were not rejected due to lack of data, 330 were identified as members with >80% confidence; the corresponding total completeness is 87%. We found that 15 stars were rejected for having inconsistent photometry, and 24 were rejected for having inconsistent proper motions. Of the

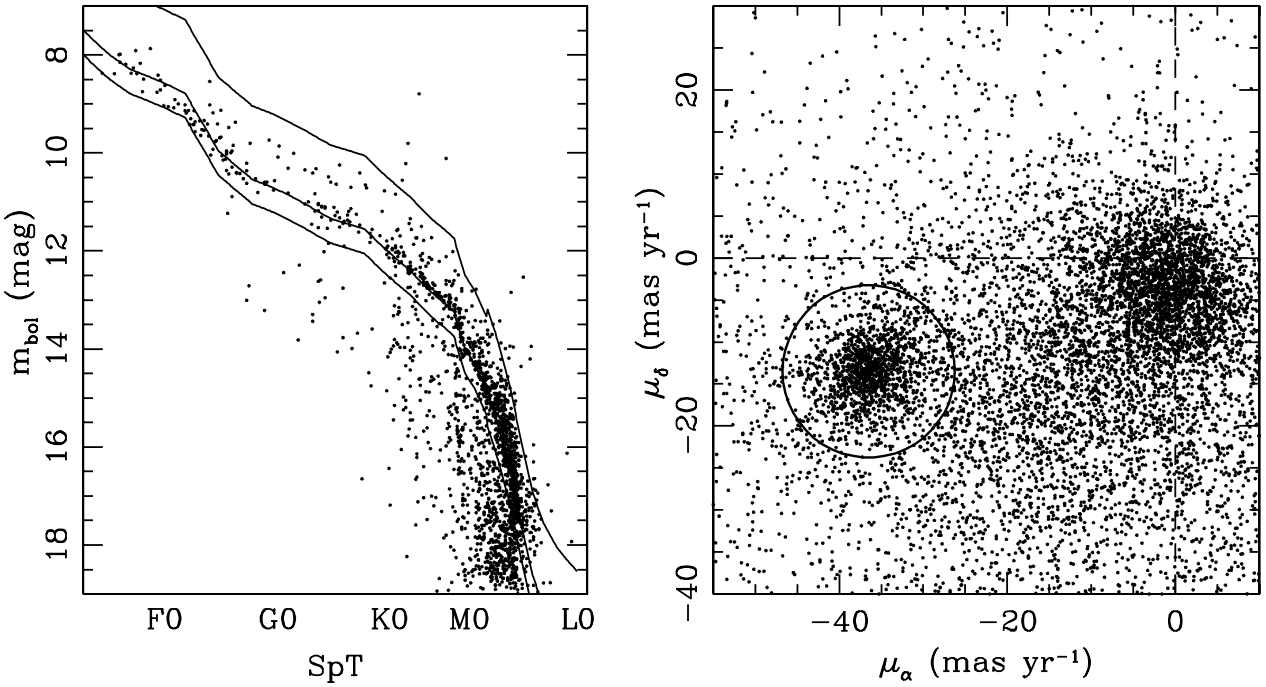

FIG. 4.—*Left*: H-R diagram for all objects which have proper motions within 8 mas yr^{-1} of the mean value for Praesepe. The field main sequence at the distance of Praesepe is shown by the middle line; the outer lines outline our photometric selection limits. We identified few candidate members of Praesepe fainter than $m_{bol} = 17.5$. The possible sequence below and blueward of this point is not a genuine feature, but is instead a result of the large number of background early- to mid-M dwarfs with similar proper motions. These stars are spatially uniformly distributed, which also argues that they are not associated with the cluster. *Right*: Proper-motion diagram for all objects which fall within our photometric selection limits. The circle outlines the 2 σ limit for a low-mass (M5) Praesepe member. [*See the electronic edition of the Journal for a color version of this figure*.]

15 stars rejected based on their photometry, 10 also possessed discrepant proper motions, suggesting that these sources are probably not genuine members of Praesepe and raising our completeness above 90%.

In Figure 6 we plot the completeness as a function of spectral type for members of Praesepe. We project that our survey is $\gtrsim$90% complete for spectral types F0–M5, declining to 0% completeness for spectral types $\leq$A5 and $\geq$M7. The incompleteness for early-type stars is a result of the bright limit of UCAC2 data, while the incompleteness for late-type stars is a result of the detection limits for USNOB and 2MASS, which are reached nearly simultaneously for stars on the Praesepe and Coma Ber cluster sequences. The low-mass limit is also consistent with the results we summarize in Table 2, since we found no members with late M spectral types.

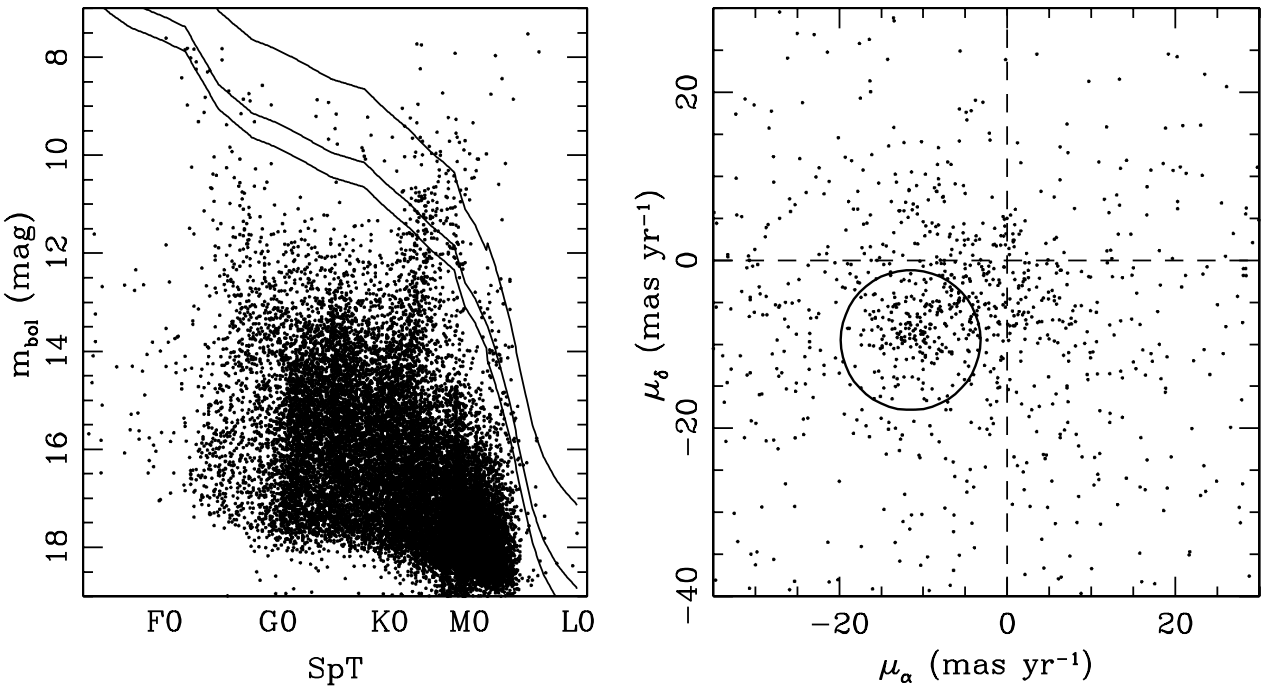

FIG. 5.—Same as Fig. 4, but for Coma Ber. [*See the electronic edition of the Journal for a color version of this figure*.]

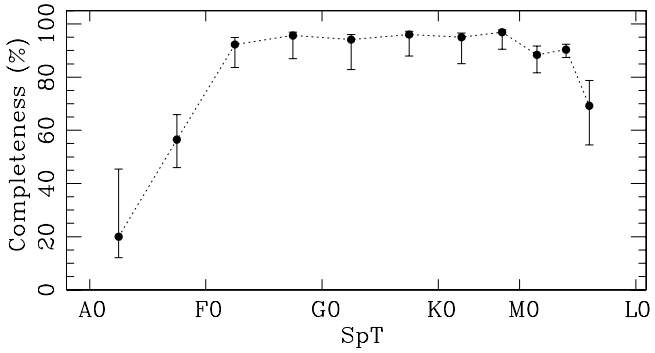

FIG. 6.—Completeness as a function of spectral type for our high-confidence sample of Praesepe members. The high-mass cutoff is a result of image saturation, while the low-mass cutoff is a result of nondetection by 2MASS and USNOB. We expect similar results for Coma Ber, but given that its members are ~1.5 mag brighter, the 90% completeness range will shift to later spectral types (F5–M6).

We project that the 90% completeness limits should be marginally later (F5 and M6) for Coma Ber, since it is closer and its members are brighter; the completeness is also lower for K stars due to contamination from background K giants.

These results are mostly consistent with our comparison to individual surveys. In Praesepe, we find excellent agreement in comparing our list of high-probability candidates with those of Jones & Stauffer (1991) and Hambly et al. (1995a); approximately 90% of each survey's high-confidence ($P_{\rm mem} > 80\%$) candidates were also identified as high-confidence candidates by our survey. We find less overlap with the Praesepe survey of Adams et al. (2002) and the Coma Ber survey of Casewell et al. (2006). Of the candidates which Adams et al. identify as "high-confidence" ($P_{\rm mem} > 20\%$ and $r < 4^\circ$), we only recovered 483 of 724 in our list of high-probability candidates. Casewell et al. used a moderately mass-dependent threshold, varying in the range $60\% < P_{\rm mem} < 90\%$, to identify 60 new candidate members. Of these stars, we only recover 22.

For both of these surveys, much of the contamination can be traced to the use of 2MASS *JHK* photometry in the color selection procedures. The $K, J - K$ color-magnitude sequence for dwarfs is nearly vertical for spectral types M0–M6, so it is difficult to distinguish a moderately brighter foreground star or moderately fainter background star from a genuine cluster member. We found that most of the unrecovered candidates were background M0–M2 stars that fall below the cluster sequence in our H-R diagrams. For the survey by Casewell et al. (2006), we also found that the recovery fraction was exceptionally low (~20%) among K stars. We attribute this to contamination from background K giants, which affected both their survey and ours. We were able to identify only 13 of the ~40 estimated K star members with high (>80%) confidence (Tables 4 and 2, respectively), suggesting that there should be only marginal overlap. Many of the candidates from the survey by Casewell et al. appear to be likely cluster members that were only identified at lower confidence ($50\% < P_{\rm mem} < 80\%$) by our survey. However, most of their remaining candidates appear to have proper motions more consistent with nonmovement than comovement, suggesting that they are background giants.

5. THE STRUCTURE AND EVOLUTION OF PRAESEPE AND COMA BER

Open clusters are thought to be the birthplaces of most stars, so cluster evolution plays a key role in setting the environment for early stellar evolution. Present-day cluster properties can be used to determine their past history and extrapolate their future lifetime; the three most important sets of properties are the spatial structure (as inferred from mass segregation), the cluster's stellar mass function, and the total cluster mass.

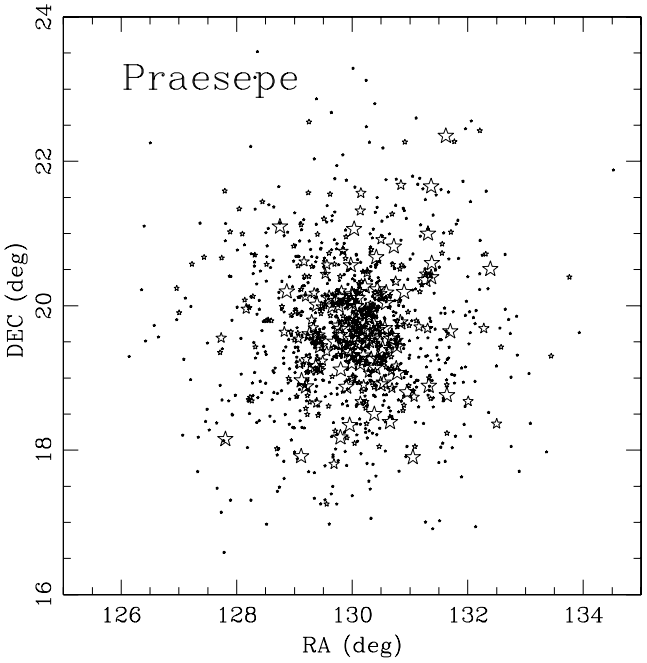

FIG. 7.—Spatial distribution of high-probability ($P_{\rm mem} > 80\%$) members of Praesepe. The points are scaled to decreasing size for A–F, G, K, and M stars.

5.1. *Radial Distributions and Mass Segregation*

In Figures 7 and 8 we plot the spatial distribution of all high-probability candidate members of Praesepe and Coma Ber. In each plot we have scaled the points to decreasing sizes for A–F, G, K, and M stars. These figures clearly illustrate the radial density profile of each cluster. However, it is perilous to infer cluster properties directly from the distribution of individual stars. The surface density as a function of radius, $\Sigma(r)$, is biased in our sample because each star's radial distance is factored into its membership probability.

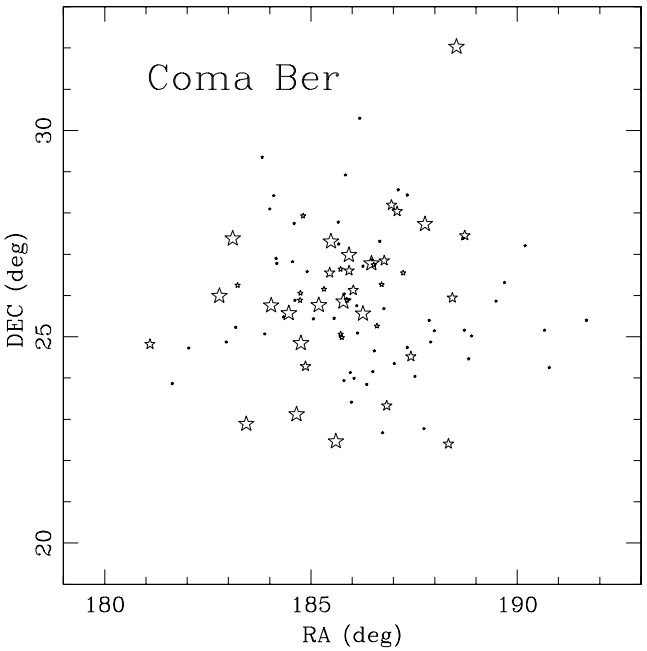

FIG. 8.—Same as Fig. 6, but for Coma Ber.

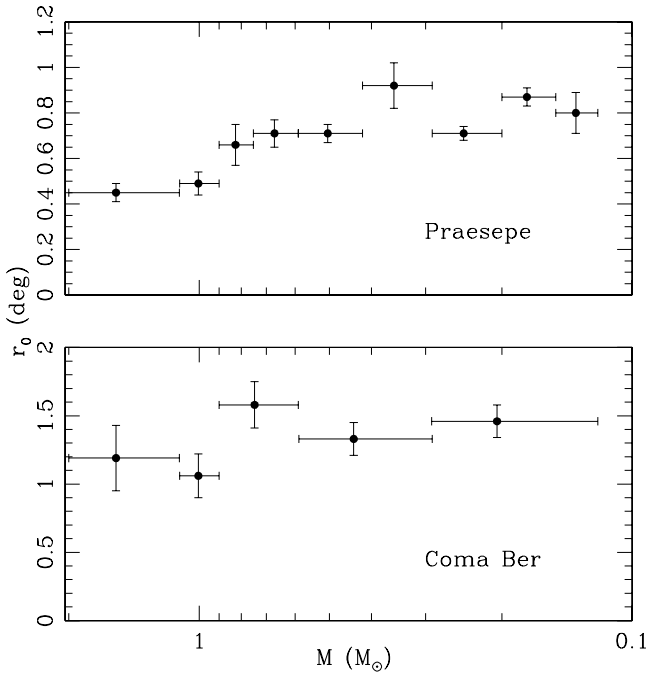

FIG. 9.—Scale radius $r_0(M)$ for each cluster. The scale radius in Praesepe clearly increases with decreasing mass, indicating the presence of mass segregation. The corresponding trend for Coma Ber is inconclusive due to low number statistics.

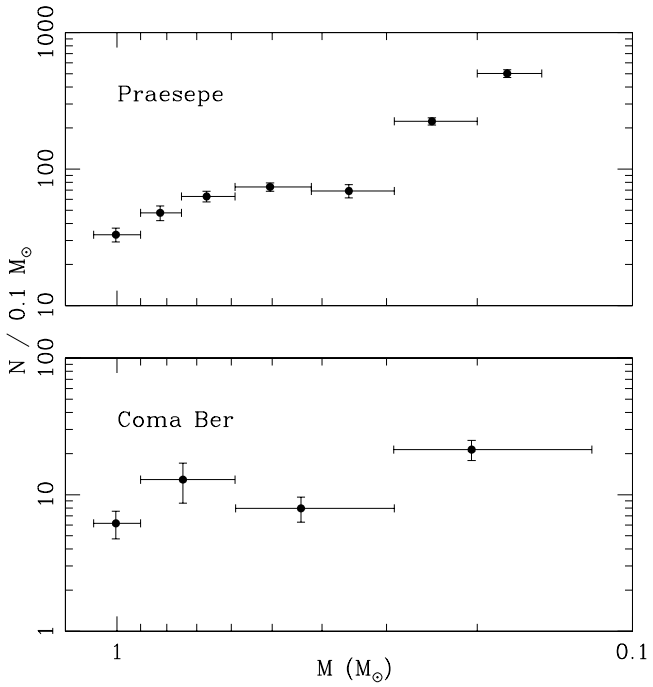

FIG. 10.—Mass functions, $\Psi(M) = dN/dM$, for Praesepe and Coma Ber. We derived these results from our best-fit values for $N_c(M)$, as described in § 3.3 and Table 2; each spectral type bin corresponds to a different width in mass, so we normalized all bins to report the number of stars per 0.1 $M_\odot$.

Ideally, cluster properties should be estimated using an unbiased method. Our parametric determination of the *e*-folding scale radius r_0 provides a natural diagnostic for quantifying the radial distribution and mass segregation of each cluster. This quantity allows us to study these properties without dependence on potentially biased measurements for individual stars, plus we can avoid arbitrary choices like the selection of a cutoff in $P_{\rm mem}$.

In Figure 9 we plot the mass-dependent function $r_0(M)$ for Praesepe (*top*) and Coma Ber (*bottom*). The uncertainties and upper limits were derived using the Monte Carlo methods described in § 3.3. As we described in § 4.2, the completeness of our sample drops for spectral types later than M5 in Praesepe and M6 in Coma Ber, so we do not plot results below these limit. In Praesepe, the scale radius increases significantly across the full mass range, following the power law $r_0 \propto M^{-0.25\pm0.06}$, which indicates the clear presence of mass segregation. Coma Ber shows no clear trend to indicate mass segregation, but the result is more uncertain: $r_0 \propto M^{-0.10\pm0.09}$. We expect Coma Ber to be less segregated than Praesepe due to its younger age and lower stellar density, but a trend with the same slope as in Praesepe is inconsistent by only $<2\ \sigma$.

5.2. *Mass Functions*

The present-day mass function provides an important test of the evolutionary state of each cluster, assuming clusters form with a common initial mass function. Dynamical evolution (mass segregation and tidal stripping) will preferentially remove low-mass cluster members, so evolved clusters should show large deficits of low-mass stars. The mass function is defined as $\Psi(M) = dN/dM$, such that $\Psi(M)$ is the number of stars with masses in the interval $(m, m + dm)$. We have constructed mass functions using the spectral type intervals defined in § 3.3, where the number of stars is the quantity N_c determined in our fitting routine. These mass bins have uneven width, so we normalized each value to represent the number of stars per 0.1 $M_\odot$ interval.

In Figure 10 we plot the cluster mass functions for Praesepe (*top*) and Coma Ber (*bottom*). Each function can be fit with a single power law, $\Psi \propto M^{-\alpha}$, where $\alpha = 1.4 \pm 0.2$ for Praesepe and $\alpha = 0.6 \pm 0.3$ in Coma Ber. Both power laws are significantly shallower than a Salpeter IMF ($\alpha = 2.35$), but the Praesepe power law agrees well with the present-day mass function for nearby field stars ($\alpha = 1.35 \pm 0.2$ for 1.0–0.1 $M_\odot$; Reid et al. 2002). Previous studies of the mass function for young clusters and unbound associations have also found similar slopes in this mass range ($\alpha \sim 1.25 \pm 0.25$; Hillenbrand 2004 and references therein).

Neither cluster has a sharp decline in the number of low-mass members within the mass range of our sample. Chappelle et al. (2005) found that the Praesepe mass function may drop sharply just below the limit of our survey ($\lesssim$0.12 $M_\odot$), which could denote the effect of tidal stripping of low-mass members, but we cannot confirm or disprove this result. The shallower power law of the Coma Ber mass function suggests that some of its low-mass members may have been removed, but it appears that any limit for the total depletion of cluster members must lie below $\sim$0.12 $M_\odot$ as well.

5.3. *Cluster Masses and Tidal Radii*

We have derived the total masses of each cluster by integrating the mass functions that we described in the previous section. Since these mass functions do not include high-mass stars, we have manually added the masses of known high-mass cluster members which were not identified in our survey, comprising $\sim$1/3 of the total mass. We identified the missing Praesepe members using our high-confidence cluster sample (§ 2.5), plus the five evolved giant members identified by Klein-Wassink (1927), while the corresponding members of Coma Ber were identified from the original member list of Trumpler (1938).

We have not included any of the candidate Coma Ber members suggested by subsequent surveys (Bounatiro 1993; Odenkirchen

et al. 1998), since it has been suggested that a significant fraction of these candidates may be spurious (Ford et al. 2001). We also did not attempt to include any substellar or near-substellar members of Praesepe or Coma Ber, since they are not thought to comprise a significant fraction of the cluster mass (e.g., Chappelle et al. 2005).

Based on this analysis, we estimate that the total stellar populations for Praesepe and Coma Ber consist of 1050 ± 30 stars earlier than M5 and 145 ± 15 stars earlier than M6, respectively. The corresponding total masses are 550 ± 40 and $112 \pm 16\,M_{\odot}$. Given these cluster masses, we can also estimate the tidal radius of each cluster:

$$r_t = \left[\frac{GM_c}{4A(A-B)}\right]^{1/3}$$

(King 1962), where A and B are the Oort constants ($A = 14.4$ km s^{-1} kpc^{-1}; $B = -12.0$ km s^{-1} kpc^{-1}; Kerr & Lynden-Bell 1986). We derive estimated tidal radii of 11.5 ± 0.3 pc ($3.5^{\circ} \pm 0.1^{\circ}$) for Praesepe and 6.8 ± 0.3 pc ($4.3^{\circ} \pm 0.2^{\circ}$) for Coma Ber. In both cases, these radii are approximately half the radius of our search area (7°). This suggests that our survey should be spatially complete for all bound members.

Finally, we note that all of these results are likely to be marginally underestimated due to unresolved stellar multiplicity. Given the typical binary frequency found for open clusters ($\sim$30%; Patience et al. 2002) and the mean mass ratio for binaries ($\sim$0.3–0.7), the magnitude of this mass underestimate should be $\sim$20%. We will address this problem in a future publication that specifically studies stellar multiplicity in both clusters.

6. SUMMARY

We have combined archival survey data from the SDSS, 2MASS, USNOB1.0, and UCAC-2.0 surveys to calculate proper motions and photometry for $\sim$5 million sources in the fields of the open clusters Praesepe and Coma Ber. Of these sources, 1010 stars in Praesepe and 98 stars in Coma Ber have been identified as candidate members with probability >80%; 442 and 61, respectively, are newly identified as high-probability candidates for the first time. We estimate that this survey is >90% complete across a wide range of spectral types (F0–M5 in Praesepe, F5–M6 in Coma Ber).

We have also investigated each cluster's mass function and the stellar mass dependence of their radii in order to quantify the role of mass segregation and tidal stripping in shaping the present-day mass function and spatial distribution. Praesepe shows clear evidence of mass segregation, but if significant tidal stripping has occurred, it has affected only members near and below the substellar boundary ($\lesssim 0.15\,M_{\odot}$). Low number statistics make it difficult to quantify the level of mass segregation in Coma Ber. The shallower slope of its mass function suggests that some mass loss has occurred, but any mass limit for total depletion of the cluster population must fall below the limit of our survey.

The authors thank John Stauffer for providing helpful feedback on the manuscript. This work makes use of data products from 2MASS, a joint project of the University of Massachusetts and IPAC/Caltech, funded by NASA and the NSF. Our research has also made use of the USNOFS Image and Catalogue Archive operated by the USNO, Flagstaff Station (http://www.nofs.navy.mil/data/fchpix/). Funding for the SDSS has been provided by the Alfred P. Sloan Foundation, the Participating Institutions, the NSF, the US Department of Energy, NASA, the Japanese Monbukagakusho, and the Max Planck Society, and the Higher Education Funding Council for England. The SDSS is managed by the Astrophysical Research Consortium for the Participating Institutions.

APPENDIX

STELLAR SED LIBRARY

There is no single source in the literature that describes all of the SED data that we require, so we compiled a preliminary set of models from a heterogeneous set of empirical observations. We then optimized these models by comparing the color-magnitude sequences to the single-star sequence of our high-confidence Praesepe sample (§ 2.5).

Luminosities and optical colors for our high-mass and intermediate-mass stellar models (spectral types B8–K7) were based on the absolute *UBV* magnitudes of Schmidt-Kaler (1982), which we converted to SDSS absolute magnitudes using the color transformations of Jester et al. (2005). We then used the optical-NIR colors ($V-K$, $J-K$, and $H-K$) of Bessell and Brett (1988) to estimate *JHK* absolute magnitudes, and converted these values to the 2MASS filter system using the NIR color transformations of Carpenter (2001). We estimated absolute bolometric magnitudes for each model using the bolometric corrections of Masana et al. (2006).

For M dwarfs (M0–L0), we based our models on the fourth-order polynomial relation of absolute *JHK* versus spectral type described by Cruz et al. (2007); they only explicitly defined this relation for spectral types later than M6, so we used 2MASS observations of stars in the CNS3 catalog (Gliese & Jahreiss 1991) and the 8 pc sample (Reid et al. 2002) to estimate the appropriate polynomial relation for M0–M5 stars. We combined these results with the $r-i$, $i-z$, and $z-J$ colors of West et al. (2005) and the $u-g$ and $g-r$ colors of Bochanski et al. (2007). We estimated absolute bolometric magnitudes using the bolometric corrections of Leggett (1992) and Leggett et al. (2002).

Finally, we optimized our set of spectral type models by comparing theoretical color-color and color-magnitude sequences to the empirical color-color and color-magnitude sequences of our sample of high-confidence Praesepe members. We found that the absolute magnitudes of our models differed from the empirical sequence at spectral types F2–F8 and at the K/M boundary, so we adjusted these absolute magnitudes to match the empirical sequences. We did not find any need to adjust the colors of any model, which suggests that any discrepancies are a result of the bolometric corrections.

In Table 5 we list our final set of spectral type models. Our fitting routine subsamples this model grid by linearly interpolating to predict values for intermediate spectral types; our final grid of models (491 in all) proceeds from B8 to L0 in steps of 0.1 subclasses, following the recent nomenclature trend to proceed directly from K5 to K7 to M0, not using subclasses K6, K8, or K9.

For high-mass stars ($\leq$F2), we directly adopted masses from the models of Schmidt-Kaler (1982). For lower mass stars, we adopted effective temperatures for each model using the dwarf temperature scales of Schmidt-Kaler (1982) (for spectral types $\leq$M0) and Luhman (1999) (for spectral types >M0). We then combined these $T_{\rm eff}$ values with the 500 Myr isochrones of Baraffe et al. (1998) to estimate stellar masses. The appropriate mixing length has been found to change with mass (Yildiz et al. 2006), so for masses $>0.6\,M_{\odot}$ we used the models with a mixing length of H_P. For masses $<0.6\,M_{\odot}$ we used the models with a mixing length of $1.9H_P$.

TABLE 5
STELLAR SEDs

Spectral Type	M_u	M_g	M_r	M_i	M_z	M_J	M_H	M_K	M_{bol}	T_{eff}	M ($M_\odot$)
B8	0.32	−0.39	−0.04	0.34	0.62	0.01	0.10	0.11	−1.00	11900	3.8
A0	1.58	0.47	0.72	1.04	1.28	0.54	0.58	0.56	0.30	9520	2.9
A2	2.41	1.22	1.39	1.65	1.87	1.12	1.15	1.12	1.10	8970	2.4
A5	3.14	1.88	1.95	2.15	2.32	1.53	1.52	1.48	1.75	8200	2.0
A7	3.47	2.21	2.23	2.40	2.55	1.75	1.71	1.66	2.08	7580	1.8
F0	3.94	2.77	2.68	2.79	2.90	2.10	2.01	1.96	2.61	7200	1.6
F2	4.23	3.10	2.96	3.04	3.13	2.32	2.20	2.14	2.89	6890	1.5
F5	5.01	3.90	3.68	3.69	3.74	2.85	2.67	2.61	3.61	6440	1.25
F8	5.76	4.60	4.29	4.26	4.28	3.31	3.08	3.01	4.24	6200	1.17
G0	6.09	4.89	4.52	4.44	4.44	3.53	3.27	3.20	4.47	6030	1.11
G2	6.35	5.07	4.65	4.54	4.51	3.64	3.38	3.30	4.60	5860	1.06
G5	6.78	5.40	4.92	4.79	4.74	3.86	3.56	3.48	4.89	5770	1.04
G8	7.55	6.03	5.50	5.32	5.25	4.31	3.95	3.86	5.30	5570	0.98
K0	8.08	6.38	5.77	5.55	5.45	4.49	4.10	4.00	5.69	5250	0.90
K2	8.89	6.94	6.23	5.94	5.80	4.80	4.35	4.24	6.08	4900	0.82
K4	9.90	7.62	6.77	6.40	6.20	5.08	4.56	4.43	6.55	4590	0.75
K5	10.36	7.98	7.03	6.59	6.35	5.20	4.64	4.51	6.68	4350	0.70
K7	11.27	8.59	7.45	6.90	6.58	5.46	4.85	4.70	6.89	4060	0.63
M0	12.46	9.90	8.50	7.83	7.46	6.04	5.37	5.18	7.60	3850	0.59
M1	13.00	10.47	9.00	8.12	7.64	6.33	5.68	5.47	7.97	3680	0.54
M2	13.66	11.36	9.76	8.73	8.15	6.73	6.09	5.86	8.44	3510	0.42
M3	14.55	12.37	10.77	9.44	8.74	7.31	6.68	6.44	9.09	3350	0.29
M4	15.83	13.55	11.99	10.48	9.64	8.10	7.49	7.22	9.92	3180	0.20
M5	17.38	15.22	13.67	11.76	10.71	9.08	8.47	8.16	11.01	3010	0.15
M6	18.71	16.56	14.99	12.98	11.88	10.15	9.50	9.16	12.06	2840	0.12
M7	19.74	17.82	16.21	13.94	12.68	10.76	10.08	9.69	12.70	2720	0.11
M8	21.05	19.40	17.60	14.83	13.21	11.19	10.46	10.03	13.13	2600	0.102
M9	21.72	19.93	18.19	15.38	13.69	11.49	10.73	10.26	13.43	2400	0.088
L0	22.33	20.98	18.48	15.85	14.01	11.76	10.96	10.44	13.69	2200	0.078

Several studies (e.g., Hillenbrand & White 2004; Lopez-Morales 2007) have found that theoretical models can underpredict masses, so these values should be considered with some caution. The most uncertain mass range is $<0.5\ M_\odot$. Observational calibrations suggest that the models underpredict masses by ∼10%–20% in the mass range of 0.2–0.5 $M_\odot$, and the models are almost completely uncalibrated for lower masses. We have addressed this problem by increasing the masses of M1 stars by 5%, M2 stars by 10%, and later type stars by 20%; these adopted values are more consistent with the observations (e.g., Lacy 1977; Delfosse et al. 1999; Creevey et al. 2005; Lopez-Morales & Ribas 2005).

We list all of the adopted values of M and T_{eff} in Table 5.

REFERENCES

Abt, H. 1986, PASP, 98, 307
Abt, H., & Levato, H. 1977, PASP, 89, 29
Adams, J., Stauffer, J., Monet, D., Skrutskie, M., & Beichman, C. 2001, AJ, 121, 2053
Adams, J., Stauffer, J., Skrutskie, M., Monet, D., Portegies Zwart, S., Janes, K., & Beichman, C. 2002, AJ, 124, 1570
Adelman-McCarthy, J., et al. 2006, ApJS, 162, 38
Allen, L., & Strom, K. 1995, AJ, 109, 1379
Argue, A., & Kenworthy, C. 1969, MNRAS, 146, 479
Artyukhina, N. 1955, Trudy Gos. Astron. Inst. Shternberga, 26, 3
———. 1966, Trudy Gos. Astron. Inst. Shternberga, 34, 181
Baraffe, I., Chabrier, G., Allard, F., & Hauschildt, P. 1998, A&A, 337, 403
Bessell, M., & Brett, J. 1988, PASP, 100, 1134
Bidelman, W. 1956, PASP, 68, 318
Bochanski, J., West, A., Hawley, S., & Covey, K. 2007, AJ, 133, 531
Bounatiro, L. 1993, A&AS, 100, 531
Bouy, H., et al. 2006, ApJ, 637, 1056
Carpenter, J. 2001, AJ, 121, 3160
Casewell, S., Jameson, R., & Dobbie, P. 2006, MNRAS, 365, 447
Chappelle, R., Pinfield, D., Steele, I., Dobbie, P., & Magazzu, A. 2005, MNRAS, 361, 1323
Corbally, C., & Garrison, R. 1986, AJ, 92, 90
Creevey, O., et al. 2005, ApJ, 625, L127
Cruz, K., et al. 2007, AJ, 133, 439
Delfosse, X., Forveille, T., Mayor, M., Burnet, M., & Perrier, C. 1999, A&A, 344, 897
Feltz, K. A., Jr. 1972, PASP, 84, 497
Ford, A., Jeffries, R., James, D., & Barnes, J. 2001, A&A, 369, 871
Francic, S. 1989, AJ, 98, 888
Gliese, W., & Jahreiss, H. 1991, Preliminary Version of the Third Catalogue of Nearby Stars (Greenbelt: NASA)
Gould, A., & Kohlmeier, J. 2004, ApJS, 152, 103
Hambly, N., Steele, I., Hawkins, M., & Jameson, R. 1995a, A&AS, 109, 29
———. 1995b, MNRAS, 273, 505
Hillenbrand, L. 2004, in The Dense Interstellar Medium in Galaxies, ed. S. Pfalzner et al. (Berlin: Springer), 601
Hillenbrand, L., & White, R. 2004, ApJ, 604, 741
Holland, K., Jameson, R., Hodgkin, S., Davies, M., & Pinfield, D. 2000, MNRAS, 319, 956
Jeffries, R. 1999, MNRAS, 304, 821
Jester, S., et al. 2005, AJ, 130, 873
Jones, B., & Cudworth, K. 1983, AJ, 88, 215
Jones, B., & Stauffer, J. 1991, AJ, 102, 1080
Kafka, S., & Honeycutt, R. 2006, AJ, 132, 1517
Kerr, F. J., & Lynden-Bell, D. 1986, MNRAS, 221, 1023
King, I. 1962, AJ, 67, 471
Klein-Wassink, W. 1927, Publ. Kapteyn Astron. Lab. Groningen 41
Lacy, C. 1977, ApJ, 218, 444
Leggett, S. 1992, ApJS, 82, 351
Leggett, S., et al. 2002, ApJ, 564, 452
Lopez-Morales, M. 2007, ApJ, 660, 732
Lopez-Morales, M., & Ribas, I. 2005, ApJ, 631, 1120
Luhman, K. 1999, ApJ, 525, 466
Masana, E., et al. 2006, A&A, 450, 735

Monet, D., et al. 2003, AJ, 125, 984
Muench, A., Lada, C., Luhman, K., Muzerolle, J., & Young, E. 2007, AJ, 134, 411
Odenkirchen, M., Soubiran, C., & Colin, J. 1998, NewA, 3, 583
Patience, J., Ghez, A., Reid, I., & Matthews, K. 2002, AJ, 123, 1570
Pier, J., Munn, J., Hindsley, R., Hennessy, G., Kent, S., Lupton, R., & Ivezic, Z. 2003, AJ, 125, 1559
Pinfield, D., Dobbie, P., Jameson, R., Steele, I., Jones, H., & Katsiyannis, A. 2003, MNRAS, 342, 1241
Pinfield, D., Hodgkin, S., Jameson, R., Cossburn, M., & von Hippel, T. 1997, MNRAS, 287, 180
Ramberg, J. 1938, Stockholm Obs. Ann., 13, 9
Reid, I. N., Gizis, J., & Hawley, S. 2002, AJ, 124, 2721
Sanders, W. 1971, A&A, 14, 226
Schmidt-Kaler, Th. 1982, in Landolt-Börnstein New Series, Group 6, Vol. 2b, ed. K. Schaifers & H.-H. Voigt (Berlin: Springer), 18
Siegler, N., et al. 2007, ApJ, 654, 580
Skrutskie, M., et al. 2006, AJ, 131, 1163
Stauffer, J., et al. 2007, ApJS, 172, 663
Stephenson, C. B. 1986, AJ, 91, 144
Taylor, B. J. 2006, AJ, 132, 2453
Trumpler, R. 1938, Lick. Obs. Bull., 18, 167
Upgren, A. 1962, AJ, 67, 37
———. 1963, AJ, 68, 194
Wang, J., Chen, L., Zhao, J., & Jiang, P. 1995, A&AS, 113, 419
West, A., Walkowicz, L., & Hawley, S. 2005, PASP, 117, 706
Williams, S., Stauffer, J., Prosser, C., & Herter, T. 1994, PASP, 106, 817
Yildiz, M., Yakut, K., Bakis, H., & Noels, A. 2006, MNRAS, 368, 1941
York, D., et al. 2000, AJ, 120, 1579
Zacharias, N., McCallon, H., Kopan, E., & Cutri, R. 2003, in 25th IAU Meeting, Joint Discussion 16, The International Celestial Reference System: Maintenance and Future Realizations, ed. R. Gaume, D. D. McCarthy, & J. Souchay (Washington: USNO), 43
Zacharias, N., Urban, S., Zacharias, M., Wycoff, G., Hall, D., Monet, D., & Rafferty, T. 2004, AJ, 127, 3043